ACS OMEGA

Article

Cite This: ACS Omega 2018, 3, 10953−10966

http://pubs.acs.org/journal/acsodf

Two Birds with One Stone: Spontaneous Size Separation and Growth Inhibition of Femtosecond Laser-Generated Surfactant-Free Metallic Nanoparticles via ex Situ SU-8 Functionalization

Dongshi Zhang,[†,◆] Wonsuk Choi,[†,‡,§,◆] Kenjiro Yazawa,[⊥] Keiji Numata,[⊥] Ayaka Tateishi,[⊥] Sung-Hak Cho,[‡,∥] Hsiu-Pen Lin,[#,∇] Yaw Kuen Li,[∇] Yoshihiro Ito,[#,○] and Koji Sugioka*[,†]

[†]RIKEN Center for Advanced Photonics, 2-1 Hirosawa, Wako, Saitama 351-0198, Japan

[‡]Department of Nano-Mechatronics, Korea University of Science and Technology (UST), 217 Gajeong-ro, Yuseong-gu, Daejeon 34113, Korea South Korea

[§]Department of Nano-Manufacturing Technology and [∥]Department of Laser & Electron Beam Application, Korea Institute of Machinery and Material (KIMM), 156 Gajeongbuk-ro, Yuseong-gu, Daejeon 34103, Republic of Korea

[⊥]Biomacromolecules Research Team, RIKEN Center for Sustainable Resource Science, 2-1 Hirosawa, Wako, Saitama 351-0198 Japan

[#]Emergent Bioengineering Materials Research Team, RIKEN Center for Emergent Matter Science, 2-1 Hirosawa, Wako, Saitama 351-0198, Japan

[∇]Department of Applied Chemistry, National Chiao Tung University, Science Building 2, 1001 Ta Hsueh Road, Hsinchu, Taiwan 300, ROC

[○]Nano Medical Engineering Laboratory, RIKEN Cluster for Pioneering Research, 2-1 Hirosawa, Wako, Saitama 351-0193, Japan

ABSTRACT: Laser ablation in liquids (LAL) offers a facile technique to develop a large variety of surfactant-free nanomaterials with high purity. However, due to the difficulty in the control of the particle synthesis process, the as-prepared nanomaterials always have a broad size distribution with a large polydispersity (σ). Surfactant-free properties can also cause problems with particle growth, which further increases the difficulty in size control of the colloids. Therefore, searching for strategies to simultaneously unify the sizes of colloids and inhibit particle growth has become significantly important for LAL-synthesized nanomaterials to be extensively used for biological, catalytic, and optical applications, in which fields particle size plays an important role. In this work, we present a facile way to simultaneously realize these two goals by ex situ SU-8 photoresist functionalization. Ag nanoparticles (NPs) synthesized by femtosecond laser ablation of silver in acetone at laser powers of 300 and 600 mW were used as starting materials. The synthesized Ag NPs have a broad size distribution between 1 and 200 nm with an average size of ca. 5.9 nm and σ of 127−207%. After ex situ SU-8 functionalization and 6 months storage, most particles larger than 10 nm become aggregates and precipitate, which makes the size distribution narrow with an average diameter of 4−5 nm and σ of 48−78%. The precipitation process is accompanied by the decrease in colloid mass from the initial ∼0.2 to 0.10−0.11 mg after ex situ SU-8 functionalization and 6 months colloid storage. Morphology analysis indicates that ex situ SU-8 functionalization inhibits the particle growth into polygonal nanocrystals. Radical polymerization of SU-8 on Ag NPs is considered to be the reason for both spontaneous size separation and growth inhibition phenomena. Benefiting from Ag NPs embedment and acetone dissolution, the glass-transition temperature of SU-8 photoresist increased from 314 to 331 °C according to thermogravimetric analysis. The universality of ex situ SU-8 functionalization-induced growth inhibition and size separation behaviors is further proved using the Au colloids generated by LAL in acetone. This work is expected to provide a new route for better size control of LAL-synthesized colloids via ex situ photoresist functionalization, although a half of colloidal mass is wasted due to radical polymerization-induced colloidal precipitation.

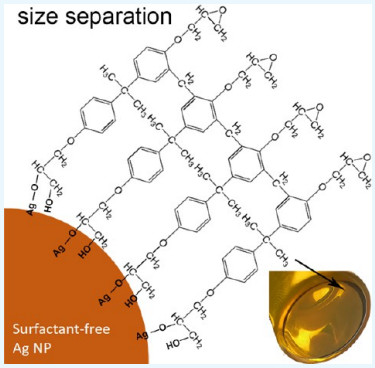

INTRODUCTION

In over last 2 decades, a newly emerged nanoscience technique known as laser ablation in liquids (LAL) has demonstrated its ability for the convenient synthesis of a large variety of nanomaterials composed of metallic, alloy, doped oxides, and particle−polymer composites.[1−7] LAL is also possible to be implemented in the presence of an external electric[8,9] or magnetic field[10,11] to produce nonspherical nanostructures.[5] Downstream treatment, such as ex situ conjugation,[3,12−14] enables researchers to construct particle−polymer or particle−

Received: June 5, 2018
Accepted: August 20, 2018
Published: September 11, 2018

DOI: 10.1021/acsomega.8b01250
ACS Omega 2018, 3, 10953−10966

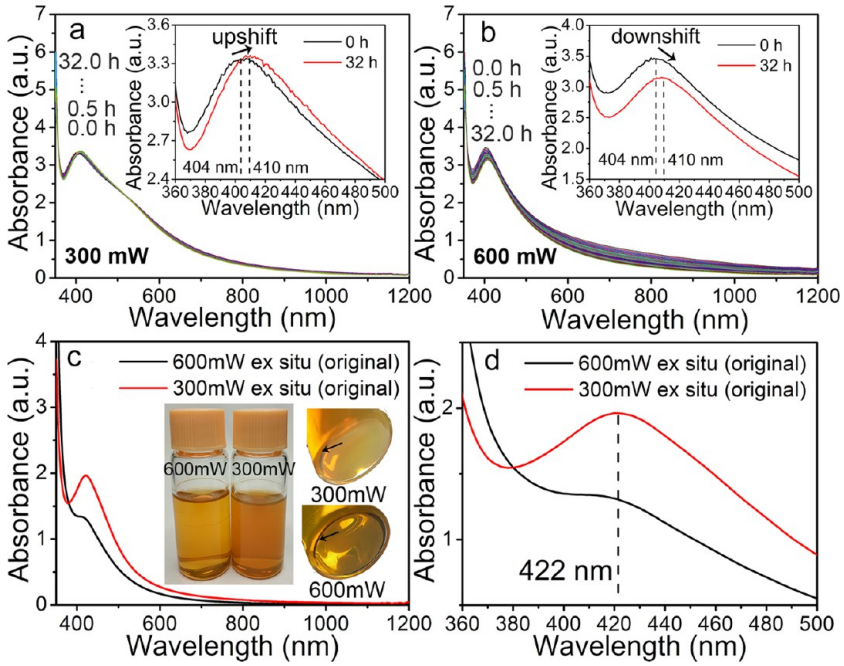

Figure 1. Absorption spectra for ex situ SU-8-functionalized Ag NPs using the Ag colloids synthesized by laser ablation of Ag in acetone and then stored for various times. Spectra of samples prepared at laser powers of (a) 300 mW and (b) 600 mW and stored within 32 h (insets: enlarged spectra in the wavelength range of 360−500 nm for the samples stored for 0 and 32 h). (c) Spectra of samples prepared at laser powers of 300 and 600 mW and then stored for 6 months (inset: photographs of aged colloids) and (d) enlarged spectra in the wavelength range of 360−500 nm. The black colloids marked by "black arrows" in (c) indicate colloidal precipitation.

biomolecule composites, respectively. Currently, the productivity of LAL has already reached 4 g/h,[15,16] almost comparable to that of wet-chemistry methods. For a long-term nanomaterial production, LAL becomes much cheaper than the wet-chemistry technique[17] so that industrial applications of LAL-generated nanomaterials in the future are envisioned, which is one of the main driving forces for the rapid expansion of LAL all over the world in recent years.[1]

In the absence of surfactants during the fabrication procedure, the as-prepared nanomaterials always possess high purity,[1] which makes them very appealing for catalytic and biological applications.[2,18−20] On the other hand, high purity also means that the surfactant-free particles suffer from spontaneous growth[21] due to colloidal Brownian collision, which leads to their evolution into different structures, such as nanocubes,[22,23] nanowires,[24,25] onion-structured spheres,[26] nanofibers, and nanosheets.[23] This issue further gives rise to the broad/bimodal size distribution problem of LAL-synthesized colloids being closely related to different mechanisms and the complex gas-phase/liquid-phase processes, involving particle nucleation and growth.[27,28]

Two options, laser modulation and surface chemistry manipulation, are available for size control of LAL-synthesized nanomaterials.[1] The former strategy is mainly implemented by changing laser parameters such as laser power,[29] pulse duration,[30] repetition rate,[31] and beam shape,[32] fragmenting particles into smaller particles,[33−35] or melting the particles into submicrospheres.[36−38] The latter strategy relies on either the conjugation of the particles by polymers[3,39] or biomolecules[40,41] or the inhibition of particle growth by salts,[42,43] surfactants,[44,45] or carbon clusters while implementing LAL in organic solvents.[46] As easily deduced, even though the particle sizes are tailored, the particles obtained by laser modulation are still surfactant-free, which inevitably induces particle growth. For example, we have recently observed that ultrasmall Ag nanoparticles (NPs) grow into polygonal nanocrystals accompanied by an increase in the particle size during storage of the colloid for 6 months.[47] Therefore, tailoring the colloidal surface chemistry by ex situ functionalization would be a better solution to accurately control the particle size. However, some problems still arise when adopting this strategy. For example, Dell'Aglio et al. observed the rapid colloidal aggregation after ex situ conjugation of ubiquitin on bare Ag NPs, which led to an obvious red shift of the colloidal surface plasmon resonance (SPR) band and a decrease in the SPR intensity.[48] A similar trend was observed by Meneghetti's group when they performed ex situ functionalization of Ag NPs with α-lipoic acid and dodecanethiol molecules.[49] Therefore, finding a suitable carrier that can not only inhibit particle growth without strong colloidal aggregation but also can bring new functions to the particles is of great importance. In this regard, photoresists that can be used to construct three-dimensional (3D) functional structures and films[50,51] are considered as good candidates for a thorough investigation. Barcikowski's group introduced LAL-synthesized Ni−Fe nanoparticles in SU-8 to linearly align the magnetic particles with the aid of an external magnetic field.[52] Jonušauskas et al. embedded LAL-synthesized Au particles inside a negative photoresist (zirconium/silicon hybrid sol−gel SZ2080) and implemented the Au NPs plasmon-assisted three-dimensional (3D) microstructuring.[53] Although SZ2080 could increase the stability of Au NPs in isopropanol for months,[53] the issues regarding how the fresh surfactant-free LAL-generated colloids behave in the presence of photoresist polymers, whether colloidal aggregation occurs, the extent to which the colloids become aggregated after ex situ polymer functionalization, and whether the aggregated colloids stay inside the liquids or precipitate over time, are still seldom studied. All of these

DOI: 10.1021/acsomega.8b01250
ACS Omega 2018, 3, 10953−10966

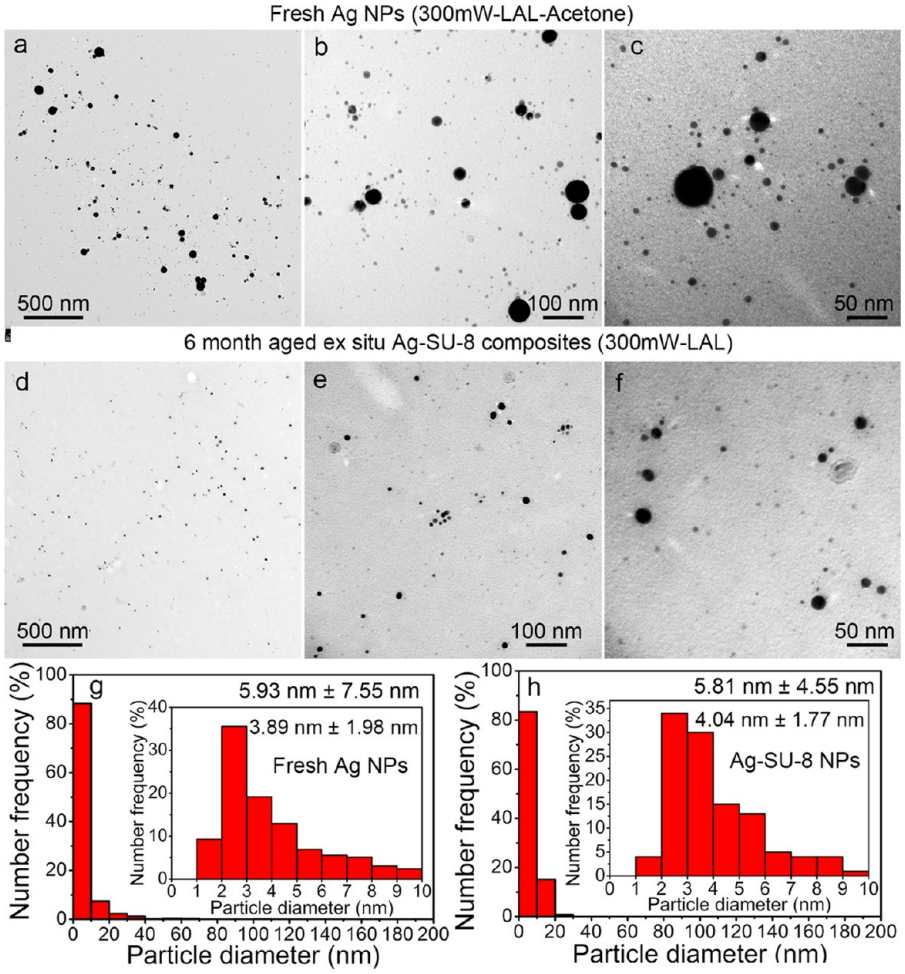

Figure 2. TEM images and size distributions of the fresh 300 mW LAL–Ag colloids (a–c, g) which was synthesized by LAL of Ag at a laser power of 300 mW and ex situ SU-8-functionalized Ag colloid (d–f, h) after storage for 6 months, respectively.

issues should be clarified to establish a steady foundation for the controllable 3D printing of particle–photoresist nanocomposites.

In this work, Ag particles freshly synthesized by femtosecond LAL in acetone at laser powers of 300 and 600 mW for 60 min were used as the starting materials. We demonstrate that ex situ photoresist SU-8 functionalization does not only spontaneously narrow the colloidal size distribution due to the precipitation of large particle aggregates, but also inhibits particle growth into polygonal crystals. The variation in the absorbance of the ex situ functionalized Ag–SU-8 composite colloids was recorded using a UV–vis spectrometer. Particle size analysis based on transmission electron microscopy (TEM) observation of the fresh Ag colloids and 6 months-aged SU-8-functionalized Ag colloids provided evidences of both the size separation and growth inhibition phenomena. Analysis of the Ag NPs surface chemistry and the surface groups of SU-8-functionalized Ag NPs by X-ray photoelectron spectroscopy (XPS) and Fourier transform infrared spectroscopy (FTIR) measurements was performed to clarify the chemical bonding between SU-8 and Ag particles. Differential scanning calorimetry–thermogravimetric analysis (DSC–TGA) was implemented to evaluate how acetone dissolution and embedded Ag NPs alter the thermal properties of the SU-8 photoresist polymer.

RESULTS AND DISCUSSION

Figure 1a–d shows the change in absorbance of the ex situ SU-8-functionalized Ag NPs within 32 h and after storage for 6 months. As the aging time increases, the SPR peak first red-shifts from 404 to 410 nm after 32 h colloidal storage and further red-shifts to 422 nm after storage of both colloids for 6 months. A difference was observed for different laser powers in that the SPR intensity of SU-8-functionalized Ag NPs changed with time. For the composite colloid produced by 300 mW LAL, the SPR peak intensity was almost unchanged within 32 h (Figure 1a), but was significantly decreased from 3.5 to 2.0 (au) after 6 months of storage (Figure 1c,d) due to the slow precipitation of Ag NPs. In contrast, the SPR intensity for 600 mW LAL quickly decreased from 3.5 to 3.2 after storage for 32 h and then further decreased to 1.3 after storage for 6 months, which indicates the rapid precipitation of Ag NPs. The initial masses of the Ag colloids in both cases were ca. 0.20 mg. After storage for 6 months, the residual masses of Ag colloids inside the liquids changed to 0.11 and 0.10 mg for 300 and 600 mW LAL colloids, suggesting almost a half of Ag colloids in weight precipitated over time. The inset of Figure 1c shows the photographs of the composite colloids stored for 6 months. Despite almost the same initial SPR peak intensity corresponding to the same initial Ag NP concentration (Figure 1a), the SU-8-functionalized Ag colloids prepared by 300 and 600 mW LAL were orange and yellow after storage for 6

DOI: 10.1021/acsomega.8b01250
ACS Omega 2018, 3, 10953–10966

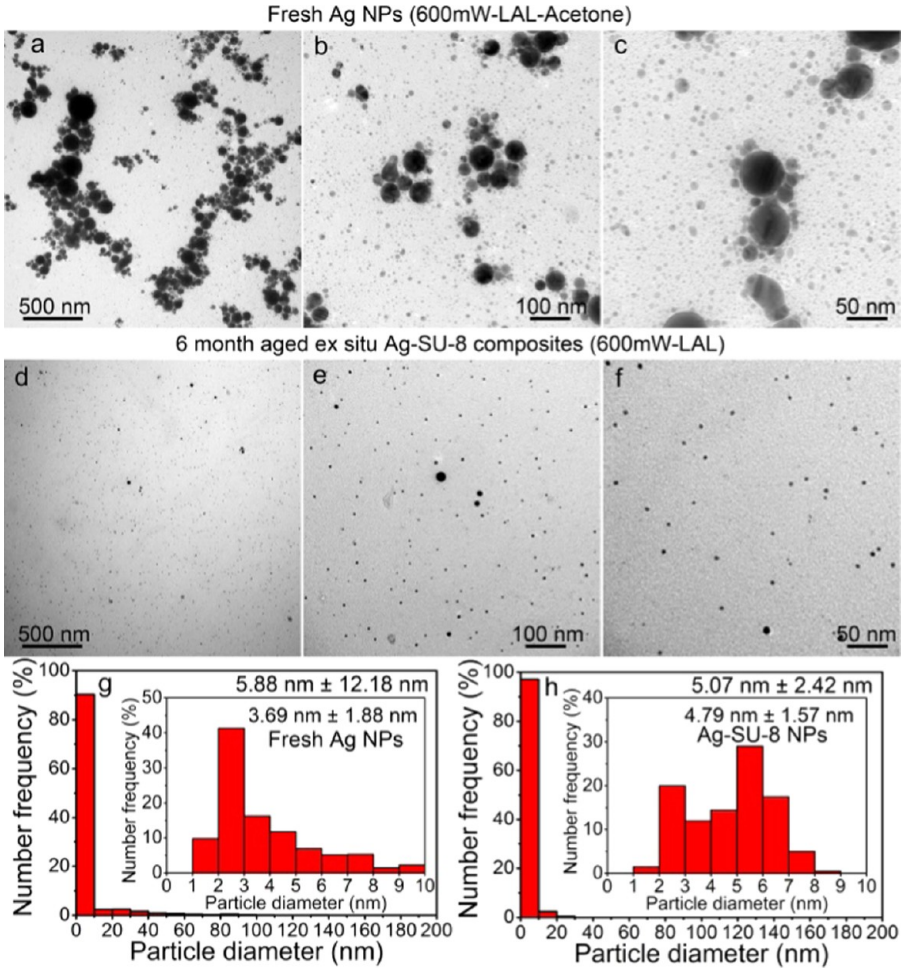

Figure 3. TEM images and size distributions of the fresh 600 mW LAL−Ag colloids (a−c, g) which was synthesized by LAL of Ag at a laser power of 600 mW and ex situ SU-8-functionalized Ag colloid (d−f, h) after storage for 6 months, respectively.

months, respectively, indicating a lower concentration of Ag NPs in the liquid for the latter case, in accordance with the SPR intensity difference shown in Figure 1d. At the bottom of the colloidal container, the precipitated particles (Figure 1c, black arrows) were clearly evident, as expected.

Figures 2a−c and 3a−c show the TEM images and the size distributions of the fresh Ag NPs synthesized by LAL at laser powers of 300 and 600 mW, respectively. The overall average sizes of the fresh 300 and 600 mW LAL−Ag NPs were 5.93 ± 7.55 nm (polydispersity (σ) = 126.7%) and 5.88 ± 12.18 nm (σ = 207.1%). Similarly to most of other LAL results,[1] the Ag colloids synthesized in this work have a broad size distribution with size variation from 1 nm to several hundred nanometers. LAL at higher laser power has higher NP productivity;[47] therefore, a larger amount of both large and small particles with diameter lower and higher than 10 nm (Figures 2a vs 3a) are generated by 600 mW LAL, and the average size of the 600 mW LAL−Ag colloid is slightly smaller than that of the 300 mW LAL colloid. Such a broad size distribution will cause a severe problem for colloidal applications such as catalysis[2] because of the difficulty in clarifying the size effect.

In our cases, small particles of 1−10 nm in diameter occupy 88 and 91% number frequency of the entire amount for 300 and 600 mW, respectively. A detailed analysis of the particle sizes in the range of 0−10 nm shows that the colloids are mainly composed of Ag clusters of ca. 2 nm in diameter (insets of Figures 2g and 3g) with average sizes of 3.89 ± 1.98 nm (σ = 50.9%) and 3.69 ± 1.88 nm (σ = 50.9%) for 300 and 60 mW, respectively, which are almost of the same size as that of metallic colloids obtained by laser fragmentation in liquids.[24] Therefore, as deduced from our experimental results, long-period femtosecond LAL in organic solvents is an attractive method to synthesize small metallic particles, as also indicated in ref 21.

The UV−vis spectra and photographs of the ex situ SU-8-functionalized Ag colloids (Figure 1) after storage for 6 months indicated a large amount of particles precipitated at the bottom of the colloidal container, while others remain stably dispersed in the solution. Analysis and comparison of the stable colloids and the precipitated particles were thus performed. Figures 2d−f and 3d−f show the morphologies of the stable Ag−SU-8 colloids after storage for 6 months. Compared to the fresh Ag colloids, which have broad size distributions, the as-aged stable ex situ SU-8-functionalized colloids have narrower size distributions. Particles larger than 30 nm were not detected. Approximately 99% number frequency of the stable particles is in the range of 1−20 nm for both cases (Figures 2h and 3h). Therefore, the spontaneous size separation phenomenon caused by large particle precipitation is evident for the ex situ SU-8-functionalized Ag colloids. The average sizes of the ex situ SU-8-functionalized 300 and 600 mW LAL−Ag NPs are 5.81 ± 4.55 nm (σ =

DOI: 10.1021/acsomega.8b01250
ACS Omega 2018, 3, 10953−10966

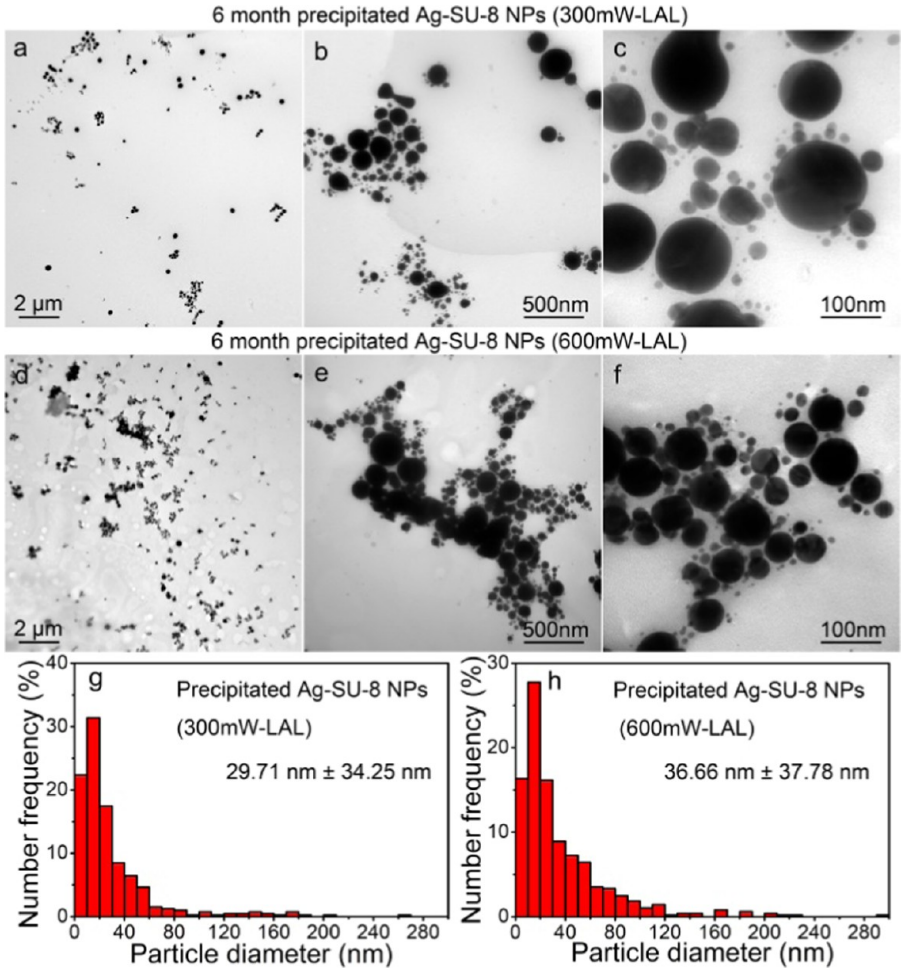

Figure 4. TEM images (a–f) and size distributions (g, h) of the precipitated ex situ functionalized SU-8–Ag composites with the colloid synthesized by LAL of Ag at laser powers of 300 mW (a–c, g) and 600 mW (d–f, h) after 6 months storage.

78.3%) and 5.07 ± 2.42 nm (σ = 47.7%), respectively, which are significantly smaller than those of the fresh Ag NPs used for ex situ functionalization and those Ag colloids stored for 6 months (7.40 ± 7.56 nm (σ = 102.2%) for 300 mW LAL and 7.82 ± 8.17 nm (σ = 104.5%) for 600 mW LAL), as shown in ref 47. Size separation phenomenon for the LAL–Ag colloids was also observed,[47] where carbon shells, carbon clusters in liquids, and self-assembled carbon sheets acted to capture large particles and resulted in precipitation. However, compared to ex situ SU-8-functionalized Ag colloids, many particles larger than 30 nm were still stable in liquids. Precipitation of lesser amounts of large Ag particles and no colloidal dilution meant that the concentrations of as-aged LAL–Ag colloids without SU-8 functionalization were much higher than those of stable SU-8-functionalized Ag after storage for 6 months, as evidenced by the SPR peak intensities after storage for 6 months (2.0 and 1.3 for ex situ SU-8-functionalized 300 and 600 mW LAL colloids, respectively (Figure 1c,d); 5.0 and 4.5 for 300 and 600 mW LAL colloids, respectively[47]). These results suggest: (1) ex situ SU-8 functionalized 600 mW LAL–Ag colloid possess higher efficiency and higher ability for size separation than the functionalized 300 mW LAL–Ag colloid; (2) ex situ SU-8 functionalization is much more efficient for size separation than the LAL colloids as evidenced by a significant decrease in the SPR peak intensity, which corresponds to stable colloidal concentrations.

The morphologies of the precipitated particle aggregates for ex situ SU-8-functionalized 300 and 600 mW LAL colloids are shown in Figure 4a–f, respectively. The maximal sizes of the aggregates are in the micrometer scale (Figure 4b,e), and these are mainly composed of particles larger than 10 nm (Figure 4g,h). The average sizes of the precipitated particles are 29.71 ± 34.25 nm (σ = 115.3%, Figure 4g) for 300 mW LAL and 36.66 ± 37.78 nm (σ = 103.1%, Figure 4h) for 600 mW LAL. As reported elsewhere,[47] Ag NPs larger than 30 nm are encapsulated by carbon shells. During the precipitation of large particles, the carbon shells should also capture a large amount of smaller Ag NPs (Figure 4c,f) to be precipitated. That is why, the precipitated particles include 22.5% (Figure 4g) and 16.5% (Figure 4h) small particles with sizes of 0–10 nm.

Although aggregation induced by ex situ functionalization significantly reduces the Ag colloidal concentrations, it facilitates the development of stable composites with narrower size distribution. Within the range of 1–10 nm, the average sizes of ex situ SU-8-functionalized Ag NPs for 300 and 600 mW LAL are 4.04 ± 1.07 nm (σ = 26.5%) and 4.79 ± 1.57 nm (σ = 32.8%), respectively. Therefore, the polydispersities of tiny Ag NPs (1–10 nm) also reduced from 50.9 to ca. 30% after ex situ SU-8 functionalization. As reported elsewhere,[47] without ex situ functionalization, the surfactant-free LAL-synthesized tiny Ag particles grow into 7–50 nm polygonal nanocrystals (Figure 5a). In contrast, the ex situ SU-8-

DOI: 10.1021/acsomega.8b01250
ACS Omega 2018, 3, 10953–10966

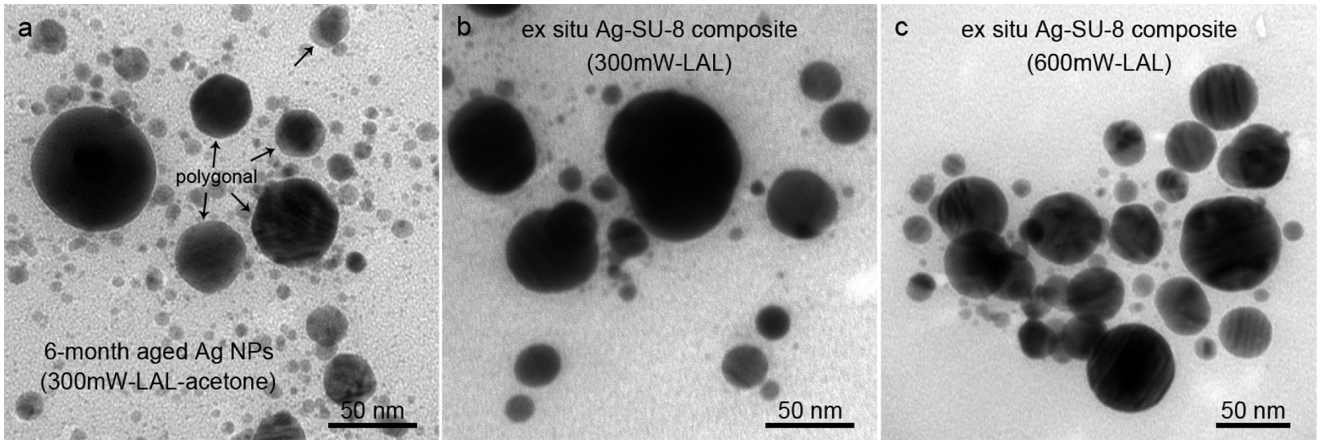

Figure 5. (a) TEM image of the Ag colloid stored for 6 months, whereby particle growth into polygonal nanocrystals occurs. (b, c) TEM images of ex situ Ag−SU-8 Ag colloids stored for 6 months, where most of Ag particles are spherical, which indicates that particle growth is inhibited by ex situ SU-8 functionalization.

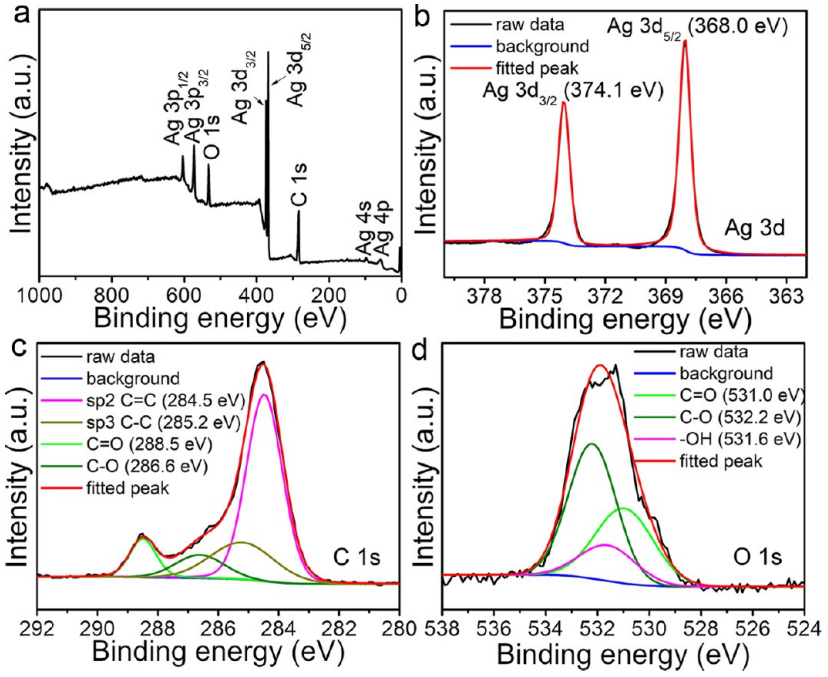

Figure 6. (a) Wide XPS scan of the Ag@C particles synthesized by laser ablation of Ag in acetone. High-resolution spectra of (b) Ag 3d, (c) C 1s, and (d) O 1s and the deconvoluted peaks.

functionalized Ag colloids are spherical in shape (Figure 5b,c). Therefore, it is reasonable to deduce that besides size separation ability, ex situ SU-8 functionalization can also inhibit the particle growth. Different from the regular Ag colloids stored for 6 months where large particles with diameters of several hundreds of nanometers are stable,[47] no such large particles are found in the six ex situ SU-8-functionalized Ag colloids stored for 6 months (Figures 2d and 3d). This means that the polymer does play an important role in the precipitation of large particles.

The surface chemistry of LAL−Ag particles was examined by XPS (Figure 6a). The percentages of Ag, C, and O quantified by XPS analysis are 16.82, 63.08, and 2.93%, indicating that the LAL-synthesized Ag particles were covered by a thick layer of carbon. The peak fit of the high-resolution C 1s spectrum by deconvolution (Figure 6c) confirmed the formation of both sp^2 C═C and sp^3 C−C, which correspond to the characteristic peaks at 284.5 and 285.2 eV.[54] The presence of sp^2 and sp^3 carbon corresponds to hybridized C−C disordered graphite and crystalline diamond or soot, respectively. The sp^2/sp^3 area ratio was calculated to be 59.29:20.00 ≈ 3:1, which indicates that the outermost surface layers of the particles are mainly covered by disordered amorphous carbon. Given that (1) the detection depth is only 5 nm for XPS characterization and (2) Ag cores can be detected by XPS, the average thickness of carbon shells is less than 5 nm. The high resolution of the XPS Ag 3d image (Figure 6b) has two peaks of Ag $3d_{5/2}$ and Ag $3d_{3/2}$ at binding energies of 368.0 and 374.1 eV, which is in good agreement with the peaks of pure Ag.[55] No other peaks corresponding to AgO (367.3 eV) or Ag_2O (367.8 eV)[56] were observed; therefore, it can be concluded that pure Ag particles are generated by femtosecond LAL of Ag in acetone. High-resolution XPS O 1s (Figure 6d) and C 1s (Figure 6c) images show that C═O carbonyl group (531. 0 eV in the O1

DOI: 10.1021/acsomega.8b01250
ACS Omega 2018, 3, 10953−10966

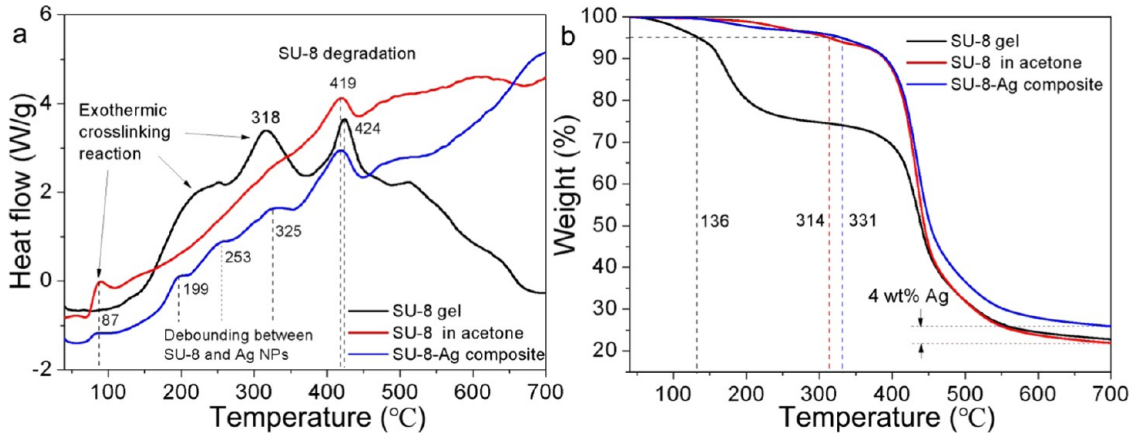

Figure 7. (a) DSC and (b) TGA analyses of SU-8 gel, acetone-dissolved SU-8 polymer, and Ag−SU-8 composites synthesized by ex situ mixing of LAL-synthesized colloids and SU-8 solution.

spectrum and 288.6 eV in the C 1s spectrum[57,58]), hydrocarbon C−O group (532.2 eV in the O 1s spectrum and 286.0 eV in the C 1s spectrum[58]), and −OH group (531.6 eV in the O 1s spectrum[59]) should conjugate the pure Ag particles. These groups originate from acetone decomposition during LAL, and their adsorption on Ag NPs endows the colloids with high stability,[60] without the need of surfactants used for wet-chemistry.

Figure 7 shows DSC and TGA images of pure SU-8 and the ex situ synthesized Ag−SU-8 composites. Two peaks are discernible in the DSC profile of pure SU-8 photoresist (Figure 7a). The peak around 87 °C is associated with the cross-linking reaction.[61] The temperature of 87 °C, at which the cross-linking reaction of SU-8 dissolved in acetone occurs, is much lower than the 120 °C for the fluorinated SU-8,[62] 220, and 318 °C for pure SU-8 gel without acetone dissolution (Figure 7a), indicating that the interaction between SU-8 and acetone has already changed the thermal properties of the SU-8 photoresist. The other peak at 419 °C for both acetone-dissolved SU-8 and SU-8−Ag composites, where rapid loss of SU-8 mass occurs, is attributed to the degradation of SU-8. In comparison, the degradation temperature of pure SU-8 gel is 424 °C, different from that (419 °C) of acetone-dissolved SU-8 and SU-8−Ag composites. Hence, it can be concluded that acetone dissolution indeed alters SU-8 molecules, especially the photoinitiator density for cross-linking actions. Compared to the pure SU-8, three new endothermic peaks are detected at 199, 253, and 325 °C for the ex situ synthesized Ag−SU-8 composites (Figure 7a, blue curve), which is ascribed to the debonding temperatures between SU-8 and Ag NPs, similar to that of polymer−Ag NP composites synthesized by other methods.[63] The bonding between SU-8 and Ag NPs alters the glass-transition temperature (T_g) of SU-8 polymer, which increases T_g from 314 °C (pure SU-8) to 331 °C after ex situ embedment of LAL−Ag NPs in SU-8, as shown in the TGA profile (Figure 7b). Both T_g values of acetone-dissolved SU-8 and SU-8−Ag composites are larger than 136 °C for pure SU-8 gel (Figure 7b), which is attributed to the significant decrease in the photoinitiator density after acetone dissolution. It is considered that the bonding between LAL−Ag NPs and SU-8 polymers changed the distribution of the polymer chain segments,[64] which partially prevents the cooperative motions necessary for the glass transition to occur. After SU-8 degradation at 700 °C, 22 wt % pyrolysate is residual, which is close to 25 wt % residue of SU-8 pyrolysate reported elsewhere.[65] Deduced from the TGA curve,[66] the Ag NP content is estimated to be 4 wt %. Epoxide rings are good synthetic intermediates; therefore, it is speculated that the epoxy groups of SU-8 should be first converted into hydroxyl groups and then act as initiator sites for the free-radical polymerization of SU-8 photoresist.[67]

To confirm this speculation, FTIR analysis of chemical groups that are conjugated on the precipitated Ag NPs was performed, and the results are shown in Figure 8. For a better

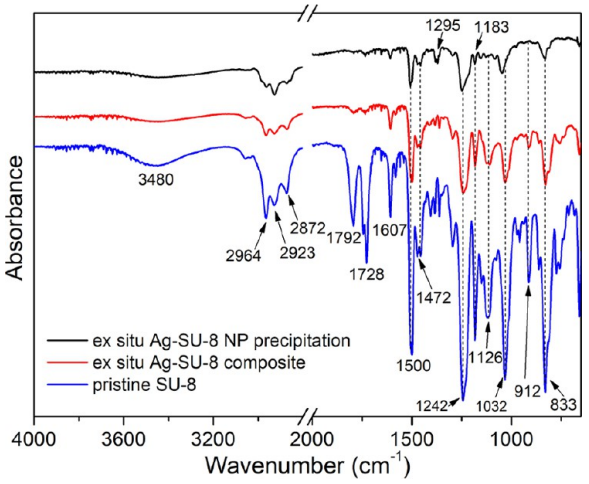

Figure 8. FTIR spectra of pristine SU-8, Ag−SU-8 composites precipitated over 6 months, and stable Ag−SU-8 colloidal composites.

understanding of how chemical groups of SU-8 change after LAL−Ag NP binding, FTIR spectra of the pristine SU-8 and ex situ synthesized Ag−SU-8 composites (from the stable colloids) are also shown (blue and red curves in Figure 8, respectively). The chemical groups, wavenumbers for different peaks, and the vibrational bindings are summarized in Table 1. The vibration bands at 1242, 833, and 912 cm^{-1} are associated with those of epoxy rings, which correspond to the C−O−C asymmetric stretch, C−O−C symmetric stretch, and CH_2−O−CH bend.[68] The band at 1295 cm^{-1} is attributed to the C−O−H stretching vibration,[69] while the bands at 1728 and 1792 cm^{-1} originate from the C═O stretching bands[70,73] of acetone molecules. The bands at 2929 and 2872 cm^{-1} are related to the symmetrical and asymmetrical stretching peaks of the $-CH_2$

DOI: 10.1021/acsomega.8b01250
ACS Omega 2018, 3, 10953−10966

Table 1. IR Absorption Modes of Pristine SU-8 and SU-8−Ag Composites

chemical group	wavenumber (cm^{-1})	assignment
epoxy rings	1242	C−O−C asymmetric stretch[68]
	833	C−O−C symmetric stretch[68]
	912	CH_2−O−CH bend[68]
benzene rings	1607	1st pair of para/ortho-substituted benzene[68]
	1500	2nd pair of para-substituted benzene[68]
	1472	2nd pair of ortho-substituted benzene[68]
ether groups	1183	−C−C−O−C− stretch[68]
	1126	−O−C−C− stretch[68]
	1032	−C−O−C− stretch[68]
others	1295	C−O−H stretch[69]
	1728, 1792	C═O stretching[70]
	2872	asymmetrical $-CH_2$ stretch[71]
	2923	symmetrical $-CH_2$ stretch[71]
	2964	CH stretch[69]
	3480	OH−[72]

groups,[71] respectively, while the 2964 cm^{-1} band is related to CH stretching.[69] The broad band at 3480 cm^{-1} can be assigned to the OH− group.[72]

As indicated from the FTIR spectra (Figure 8 and Table 1), no CH_2−O−CH band of epoxy rings was detected from the precipitated Ag NPs, while the C−O−H group appears, both of which indicate the free-radical polymerization of SU-8 photoresist with Ag NPs according to the scheme shown in Figure 9. The radicals are due to acetone decomposition during LAL.[1] Higher amounts of radicals are generated by LAL at a higher power, which explains why the ex situ functionalized 600 mW LAL−Ag NPs undergo a quicker precipitation while ex situ functionalized 300 mW LAL−Ag NPs undergo a slow precipitation (Figure 1). The preservation of epoxy rings for the stable ex situ Ag−SU-8 composites, despite the low concentration, means that polymerization of the composites could also occur similarly to that of pristine SU-8 for the construction of 3D structures or functional SU-8 composite films, which will be examined in our future work. The red shift of the SPR band has been attributed to variation of the surface chemistry[53] or an increase of the particle size.[74] In the present case, due to the decrease in the Ag particle size after colloidal storage for 6 months (Figures 2d−f and 3d−f), it can be concluded that alteration of the surface chemistry of Ag NPs caused by ex situ SU-8 functionalization leads to the red shift of the SPR band of the Ag colloids from 404 to 422 nm (Figure 1). Due to surface chemistry alternation,[75] the hydrodynamic diameters of the SU-8-functionalized Ag NPs significantly increased to 187.6 ± 41.2 (Figure 10a) and 254.6 ± 61.1 nm (Figure 10b) after 6 months storage. The larger hydrodynamic sizes and broader hydrodynamic size distributions of Ag−SU-8 composites using 600 mW LAL−Ag colloids should be attributed to higher amounts or stronger bindings of SU-8 molecules on Ag NPs originating from more radicals generated during 600 mW LAL.

To demonstrate the universality of simultaneous particle growth inhibition and size separation phenomena induced by spontaneous radical polymerization after ex situ SU-8 functionalization, the absorbance difference between 3 weeks-aged Au colloid synthesized by LAL in acetone and the Au colloid ex situ functionalized by SU-8 is shown in Figure 11 for comparison. Similarly to the case of Ag colloids shown in Figure 1, the SPR intensity of SU-8-functionalized Au colloid significantly decreases from 2.3 to 0.4 after 3 weeks storage. In comparison, the SPR intensity of 3 weeks-aged Au colloid without SU-8 functionalization slightly increases from 2.3 to 2.7 due to acetone volatilization-induced AuNP concentration increase. That is why, the optical transparency of the aged Au and SU-8−Au colloids is very different, as indicated by the inset optical images in Figure 11a. After 3 weeks storage, the SPR peak positions of Au colloid and the SU-8−Au composite colloid shift from 531 to 533 and 537 nm, respectively, indicating the particle growth of Au particles during storage and the surface alteration of Au particles after SU-8 functionalization, respectively. Figure 12 shows the TEM images of the Au colloid (Figure 12a−c) and SU-8-functionalized Au colloid (Figure 12d−f) and the calculated size distributions (Figure 12g,h). As clearly shown, the aged Au colloid has large particles with maximal size up to 87 nm, while in comparison, the maximal size of SU-8-functionalized supernatant Au colloid after 3 weeks storage is only 25 nm. Many polygonal Au particles are found from the aged Au

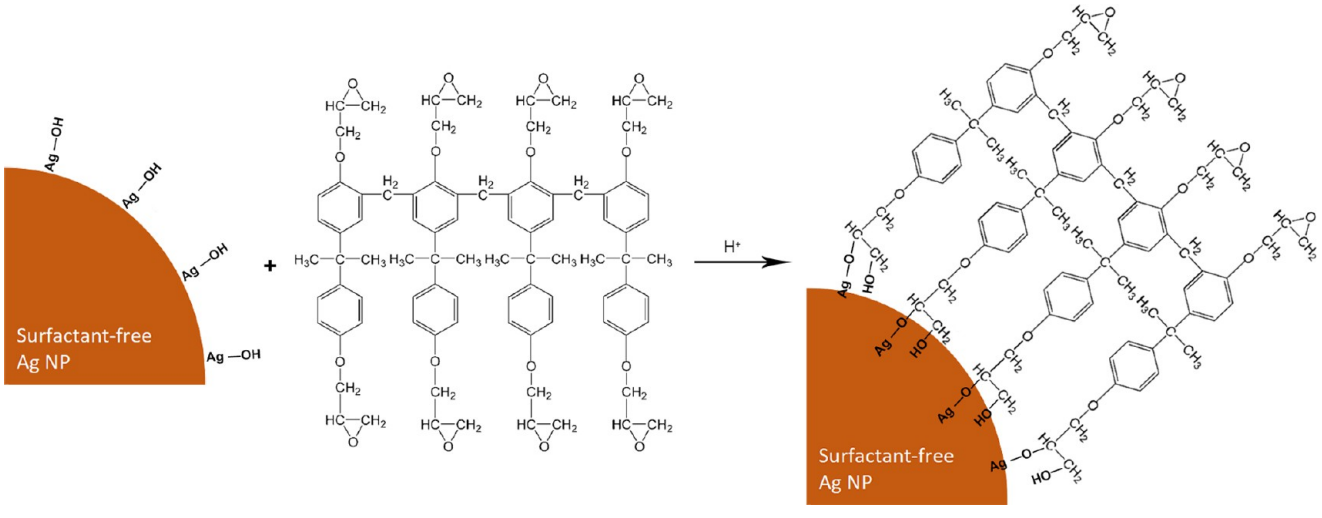

Figure 9. Scheme for the free-radical polymerization of SU-8 on surfactant-free Ag NPs.

DOI: 10.1021/acsomega.8b01250
ACS Omega 2018, 3, 10953−10966

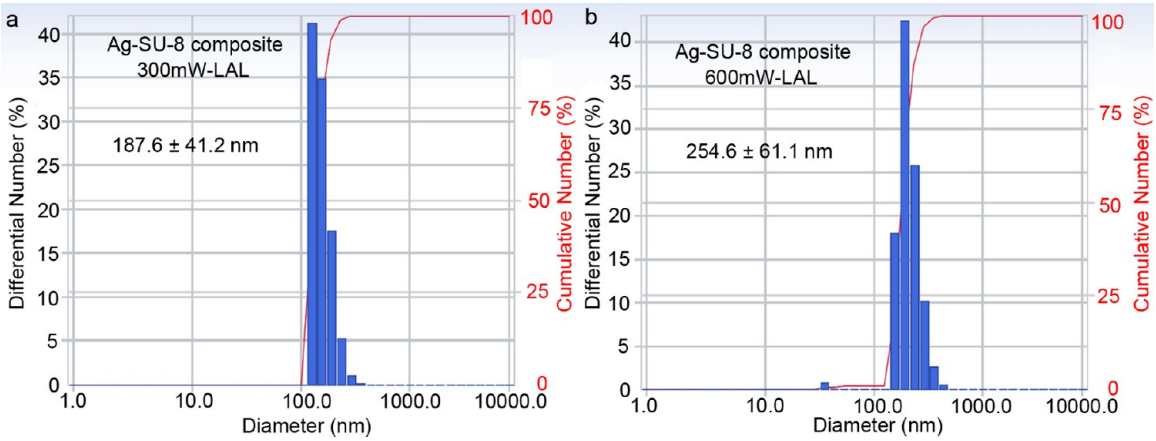

Figure 10. Hydrodynamic diameter of the SU-8-functionalized Ag composite colloids with the colloid synthesized by LAL of Ag in acetone at laser powers of (a) 300 mW and (b) 600 mW.

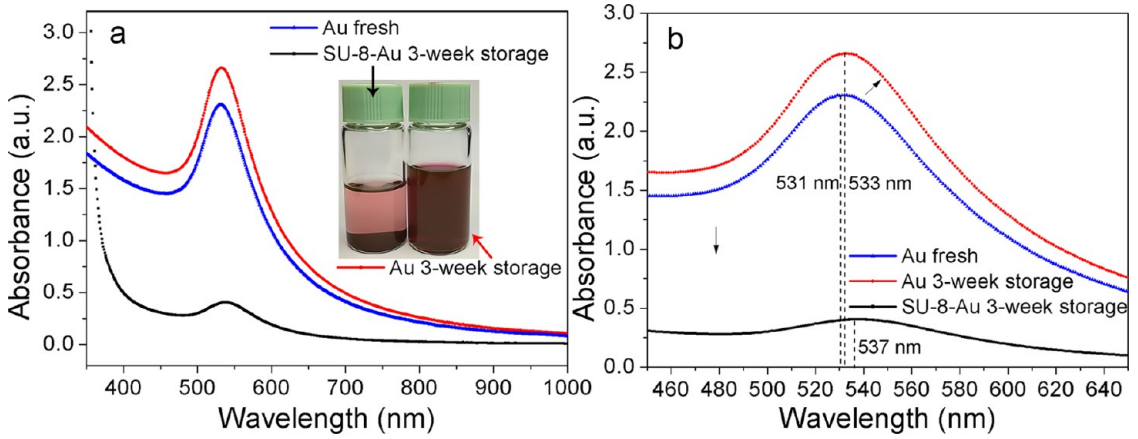

Figure 11. (a) Absorption spectra for ex situ SU-8-functionalized Au NPs using the Au colloids synthesized by LAL of Au in acetone at a laser power of 600 mW and stored for 3 weeks (inset: photographs of 3 weeks-aged Au colloid and aged SU-8−Au colloids). (b) Enlarged spectra in the wavelength range of 450−650 nm for the Au colloid and aged SU-8−Au colloids stored for 0 and 3 weeks.

colloid (Figure 13a) but seldom found from the SU-8-functionalized Au colloid (Figure 13b). This phenomenon indicates that SU-8 functionalization indeed inhibits the particle growth, which can also be deduced from the smaller average sizes of SU-8-functionalized Au particles in the range of 0−10 nm (Figure 12g,h; 3.98 ± 1.62 and 3.66 ± 1.54 nm for aged Au particles and SU-8-functionalized Au particles, respectively). Taking together, the above-mentioned findings give an evidence that radical polymerization between SU-8 molecules and LAL-generated Au particles causes the precipitation of large particles and inhibits the particle growth, similarly to the case of ex situ SU-8-functionalized Ag colloids. Recently, we have shown that the carbon clusters and the carbon shells of metal particles can behave as captors to capture large particles to become nanoaggregates and make them precipitate over time.[47] The precipitation of Au colloids also occurred during the storage. Due to similarity to Ag colloids, analysis of the precipitated Au particles was not performed in this work. In both cases, many large particles are still stable in the liquids even after storage for 6 months. In contrast, the size separation ability of ex situ SU-8 photoresist functionalization is more efficient in spite of severe colloid precipitation.

CONCLUSIONS

This work has demonstrated that ex situ SU-8 functionalization of surfactant-free Ag NPs not only allows the size selection of small particles, but also enables the inhibition of particle growth into polygonal nanocrystals. Spontaneous aggregation and precipitation of the large particles with diameters of 10−300 nm occurred during long-term storage for 6 months, irrespective of the initial amount of the large particles synthesized by LAL at laser powers of 300 and 600 mW. The colloidal concentrations thus significantly decreased, and the size distributions of the colloids narrowed with the polydispersity of the overall sizes changing from initial 126−207 to final 50−80%. As for the predominantly small (1−10 nm) particles with average sizes of 4−5 nm that occupied 82−96% number frequency of the stable SU-8-functionalized Ag NPs, the polydispersity decreased from 50.9 to 26.5−32.8%. XPS and FTIR joint analysis confirmed free-radical polymerization of SU-8 on surfactant-free Ag NPs, which is considered to be the underlying mechanism for both spontaneous size separation and growth inhibition phenomena. The acetone dissolution and the interaction between the SU-8 molecules and surfactant-free LAL-generated Ag NPs also altered the thermal properties of SU-8 photoresist. Three new endothermic peaks (199, 253, and 419 °C) were observed in the DSC curve, while the glass-transition temperature of SU-8 increased

DOI: 10.1021/acsomega.8b01250
ACS Omega 2018, 3, 10953−10966

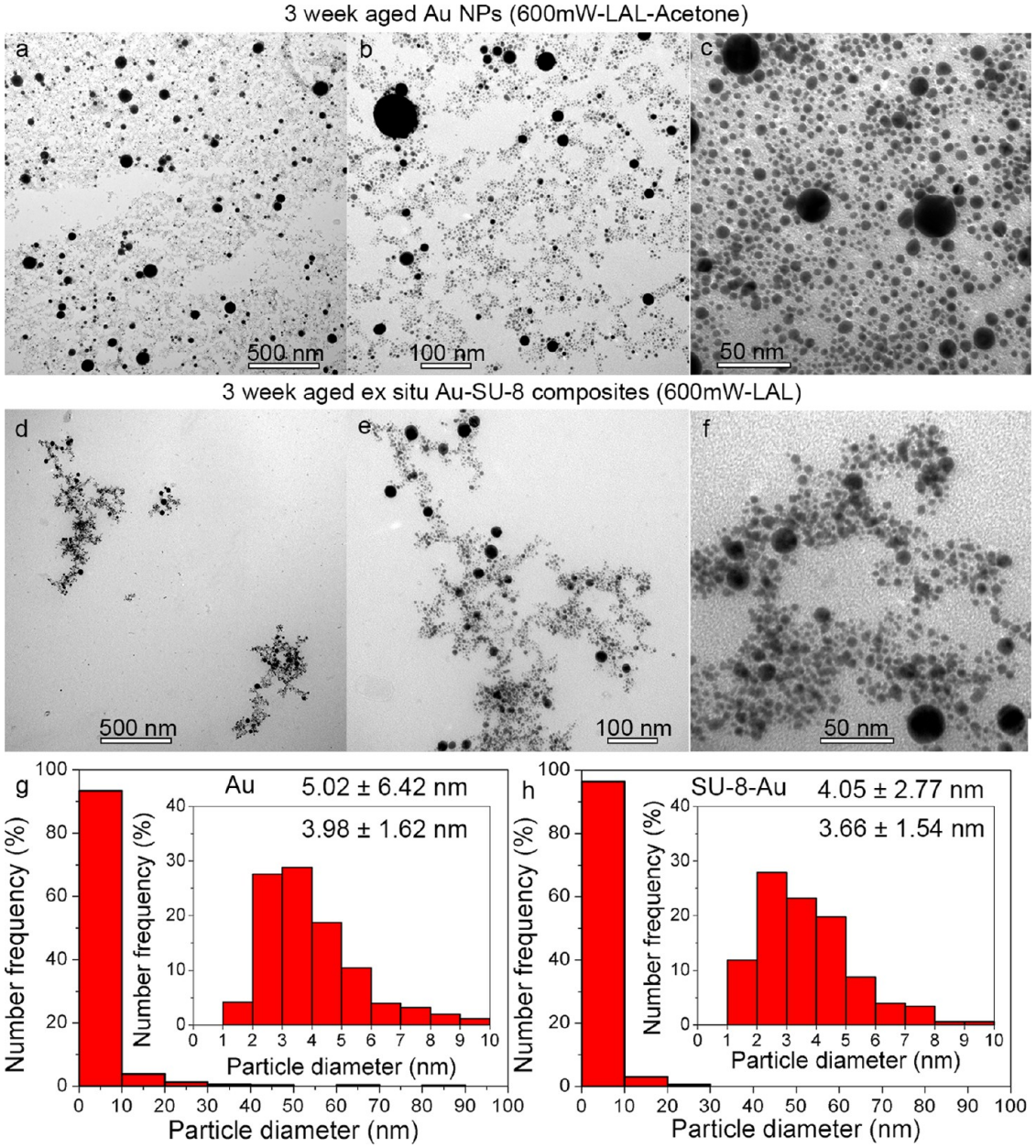

Figure 12. TEM images and size distributions of the 3 weeks-aged 600 mW LAL−Au colloid (a−c, g) and 3 weeks-aged ex situ SU-8-functionalized Au colloid (d−f, h), respectively.

from 314 to 331 °C when the ex situ SU-8-functionalized Ag NP was ca. 4 wt % of the overall weight of the composites. Successful narrowing of the size distribution of metallic colloids by ex situ photoresist functionalization and long-term storage may offer a solution to solve the broad size distribution problem of LAL colloids. It is noteworthy that if adopting this method for size control, precipitation-induced decrease in the colloid concentration will significantly lower the mass for practical applications.

METHODS

Silver colloids were synthesized by laser ablation of Ag in acetone for approximately 60 min using a femtosecond laser (FGPA μ Jewel D-1000-UG3, IMRA America Inc., Ann Arbor, MI) with pulse duration, wavelength, and repetition rate of 457 fs, 1045 nm, and 100 kHz, respectively. Two laser powers of 300 and 600 mW were adopted for LAL. A 20 mm diameter and 1 mm thick silver plate was placed inside a glass dish (45 mm diameter and 18 mm height) filled with 8 mL of acetone for LAL. A 10 mm diameter and 5 mm thick gold target was placed inside a smaller glass dish (35 mm diameter and 15 mm height) filled with 8 mL of acetone for LAL. The thickness of the liquid was approximately 5 mm above the target surface. The femtosecond laser beam was focused on the Ag plate surface using a 20× objective lens (numerical aperture = 0.4, Mitutoyo, Japan). An area of 3.5 × 3.5 mm^2 was scanned at a scan speed of 1 mm/s. The parallel-line scanning method described in refs 76−78 was adopted with an adjacent line interval of 5 μm. After synthesis, the colloids were directly mixed with the acetone-dissolved SU-8 (SU-8 2050, Micro-Chem) polymer solutions to make the weight ratio of Ag or Au colloids (including the acetone solvent used for LAL) occupy 12 wt % of the mixed solution. The colloids were stored and sealed in a glass container at room temperature. After storage

DOI: 10.1021/acsomega.8b01250
ACS Omega 2018, 3, 10953−10966

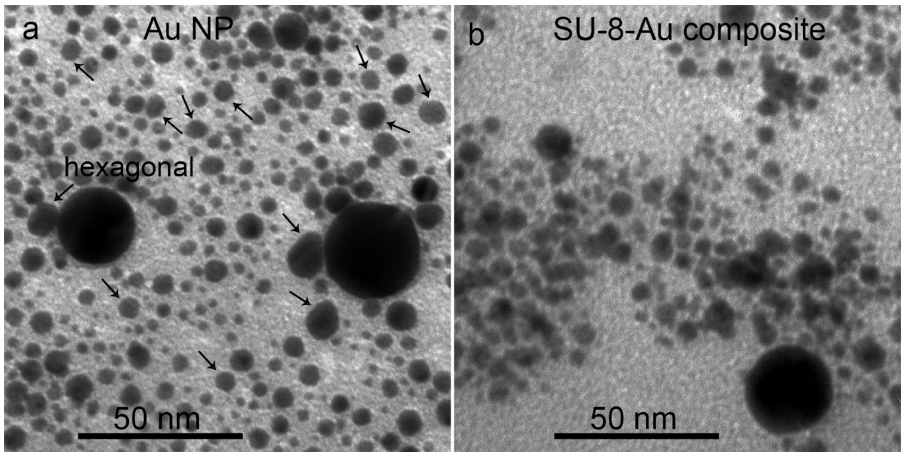

Figure 13. (a, b) High-magnification TEM images of the 3 weeks-aged Au particles and SU-8-functionalized Au composite particles, respectively. The black arrows in (a) indicates the formation of nonspherical nanostructures.

for 6 months, both the colloids in the liquids and the precipitated particles at the bottom of the glass container were characterized by TEM and UV−vis spectroscopy. The masses of the synthesized Ag colloids obtained by LAL at 300 and 600 mW were measured by comparing the weight of the Ag target before and after LAL. The residual masses of stable supernatant Ag colloids after 6 months storage were estimated by comparing the peak intensity of the fresh Ag colloids diluted by acetone with different volume ratios. The residual weight ratios of supernatant SU-8−Ag composite colloids and acetone solvents after 6 months storage in both cases were measured by comparing the weight of glass slides used for composite film deposition, the weight of the colloid used for film deposition, and the glass slides with dried SU-8−Ag composite films. The weight ratios of acetone in both supernatant SU-8−Ag composite colloids, which were stored for 6 months, were ca. 89 wt %.

Transmission electron microscope (Jeol JEM-1230) and UV−vis spectrometer (Shimadzu UV-3600 Plus) were used to characterize the morphologies of Ag NPs and Ag−SU-8 composites and record the variation in the absorption spectra of composite over time. For XPS (Rigaku SmartLab-R 3 kW) characterization, the colloids were centrifuged by a centrifuge (Eppendorf Centrifuge 5430, Germany) at a rotation speed of 14 000 rpm for 10 min and then deposited on the glass substrates. The surface chemistry of the Ag particles was analyzed by FTIR spectrometer (Shimadzu, Prestige-21). The Ag NPs precipitated at the bottom of the container were separated from the stable composite colloids and then washed twice with acetone. After each washing, the precipitated colloids were centrifuged and separated from the upper solutions to ensure that the remaining SU-8 in the liquid was removed from the precipitated Ag NPs. Then, the precipitated Ag−SU-8 composites were then directly used for FTIR characterization. For DSC−TGA (Mettler Toledo, TGA/DSC2, Greifensee, Switzerland) and FTIR characterization of the acetone-dissolved pure SU-8 and the ex situ functionalized Ag−SU-8 composites, the solutions were deposited on glass substrates and then dried in an oven at 60 °C for 10 h. The DSC−TGA measurement of pure SU-8 gel without acetone dissolution was also performed for comparison. DSC−TGA measurements were implemented in nitrogen gas at a heating rate of 20 °C every 5 min. After solidification, small pieces of the dried SU-8 and Ag−SU-8 composite films were peeled off from the glass and used for FTIR characterization. A particle size analyzer (ELSZ-2PL, Photal, Osaka, Japan) was used to measure the hydrodynamic diameters of 6 months-aged SU-8-functionalized Ag particles.

AUTHOR INFORMATION

Corresponding Author

*E-mail: ksugioka@riken.jp.

ORCID

Keiji Numata: 0000-0003-2199-7420
Yoshihiro Ito: 0000-0002-1154-253X
Koji Sugioka: 0000-0001-5833-1118

Author Contributions

◆D.Z. and W.C. contributed equally to this work.

Author Contributions

D.Z. and K.S. conceived and designed the experiments. W.C. performed the experiments. D.Z. characterized the particles and analyzed the data. K.Y., A.T., and K.N. performed the TGA−DSC measurement. H.-P.L., Y.K.L., and Y.I. performed the DLS measurement. D.Z. wrote the paper, and all authors read and revised it. The manuscript was written through contributions of all authors. All authors have given approval to the final version of the manuscript.

Notes

The authors declare no competing financial interest.

ACKNOWLEDGMENTS

The authors acknowledge Materials Characterization Support Unit, RIKEN CEMS, for providing access to the SEM and TEM devices and the XPS and FTIR spectrometers.

REFERENCES

(1) Zhang, D.; Gökce, B.; Barcikowski, S. Laser Synthesis and Processing of Colloids: Fundamentals and Applications. *Chem. Rev.* **2017**, *117*, 3990−4103.

(2) Zhang, D.; Liu, J.; Li, P.; Tian, Z.; Liang, C. Recent Advances in Surfactant-Free, Surface Charged and Defect-Rich Catalysts Developed by Laser Ablation and Processing in Liquids. *ChemNanoMat* **2017**, *3*, 512−533.

(3) Zhang, D.; Gökce, B. Perspective of laser-prototyping nanoparticle−polymer composites. *Appl. Surf. Sci.* **2017**, *392*, 991−1003.

(4) Amendola, V.; Meneghetti, M. What controls the composition and the structure of nanomaterials generated by laser ablation in liquid solution? *Phys. Chem. Chem. Phys.* **2013**, *15*, 3027−3046.

DOI: 10.1021/acsomega.8b01250
ACS Omega 2018, 3, 10953−10966

(5) Xiao, J.; Liu, P.; Wang, C. X.; Yang, G. W. External field-assisted laser ablation in liquid: an efficient strategy for nanocrystal synthesis and nanostructure assembly. *Prog. Mater. Sci.* **2017**, *87*, 140−220.
(6) Zeng, H.; Du, X. W.; Singh, S. C.; Kulinich, S. A.; Yang, S.; He, J.; Cai, W. Nanomaterials via Laser Ablation/Irradiation in Liquid: A Review. *Adv. Funct. Mater.* **2012**, *22*, 1333−1353.
(7) Yang, G. W. Laser Ablation in Liquids: Applications in the Synthesis of Nanocrystals. *Prog. Mater. Sci.* **2007**, *52*, 648−698.
(8) Liu, P.; Liang, Y.; Lin, X.; Wang, C.; Yang, G. A General Strategy To Fabricate Simple Polyoxometalate Nanostructures: Electrochemistry-Assisted Laser Ablation in Liquid. *ACS Nano* **2011**, *5*, 4748−4755.
(9) Compagnini, G.; Sinatra, M.; Russo, P.; Messina, G. C.; Puglisi, O.; Scalese, S. Deposition of few layer graphene nanowalls at the electrodes during electric field-assisted laser ablation of carbon in water. *Carbon* **2012**, *50*, 2362−2365.
(10) Liang, Y.; Liu, P.; Xiao, J.; Li, H.; Wang, C.; Yang, G. A microfibre assembly of an iron-carbon composite with giant magnetisation. *Sci. Rep.* **2013**, *3*, No. 3051.
(11) Liang, Y.; Liu, P.; Yang, G. Fabrication of One-Dimensional Chain of Iron-Based Bimetallic Alloying Nanoparticles with Unique Magnetizations. *Cryst. Growth Des.* **2014**, *14*, 5847−5855.
(12) Barchanski, A.; Taylor, U.; Klein, S.; Petersen, S.; Rath, D.; Barcikowski, S. Golden Perspective: Application of Laser-Generated Gold Nanoparticle Conjugates in Reproductive Biology. *Reprod. Domest. Anim.* **2011**, *46*, 42−52.
(13) Petersen, S.; Barcikowski, S. In Situ Bioconjugation: Single Step Approach to Tailored Nanoparticle-Bioconjugates by Ultrashort Pulsed Laser Ablation. *Adv. Funct. Mater.* **2009**, *19*, 1167−1172.
(14) Barcikowski, S.; Baranowski, T.; Durmus, Y.; Wiedwald, U.; Gökce, B. Solid solution magnetic FeNi nanostrand−polymer composites by connecting-coarsening assembly. *J. Mater. Chem. C* **2015**, *3*, 10699−10704.
(15) Streubel, R.; Barcikowski, S.; Gökce, B. Continuous multigram nanoparticle synthesis by high-power, high-repetition-rate ultrafast laser ablation in liquids. *Opt. Lett.* **2016**, *41*, 1486−1489.
(16) Streubel, R.; Bendt, G.; Gökce, B. Pilot-scale synthesis of metal nanoparticles by high-speed pulsed laser ablation in liquids. *Nanotechnology* **2016**, *27*, No. 205602.
(17) Jendrzej, S.; Gökce, B.; Epple, M.; Barcikowski, S. How Size Determines the Value of Gold: Economic Aspects of Wet Chemical and Laser-Based Metal Colloid Synthesis. *ChemPhysChem* **2017**, *18*, 1012−1019.
(18) Zhang, J.; Chen, G.; Chaker, M.; Rosei, F.; Ma, D. Gold Nanoparticle Decorated Ceria Nanotubes with Significantly High Catalytic Activity for the Reduction of Nitrophenol and Mechanism Study. *Appl. Catal., B* **2013**, *132−133*, 107−115.
(19) Hebié, S.; Holade, Y.; Maximova, K.; Sentis, M.; Delaporte, P.; Kokoh, K. B.; Napporn, T. W.; Kabashin, A. V. Advanced Electrocatalysts on the Basis of Bare Au Nanomaterials for Biofuel Cell Applications. *ACS Catal.* **2015**, *5*, 6489−6496.
(20) Zhang, J.; Chaker, M.; Ma, D. Pulsed laser ablation based synthesis of colloidal metal nanoparticles for catalytic applications. *J. Colloid Interface Sci.* **2017**, *489*, 138−149.
(21) Zhang, D.; Liu, J.; Liang, C. Perspective on how laser-ablated particles grow in liquids. *Sci. China: Phys., Mech. Astron.* **2017**, *60*, No. 074201.
(22) Liu, P.; Cao, Y. L.; Wang, C. X.; Chen, X. Y.; Yang, G. W. Micro- and Nanocubes of Carbon with C8-like and Blue Luminescence. *Nano Lett.* **2008**, *8*, 2570−2575.
(23) Zhang, D.; Ma, Z.; Spasova, M.; Yelsukova, A. E.; Lu, S.; Farle, M.; Wiedwald, U.; Gökce, B. Formation mechanism of laser-synthesized iron-manganese alloy nanoparticles, manganese oxide nanosheets and nanofibers. *Part. Part. Syst. Charact.* **2017**, *34*, No. 1600225.
(24) Jendrzej, S.; Gökce, B.; Amendola, V.; Barcikowski, S. Barrierless Growth of Precursor-Free, Ultrafast Laser-Fragmented Noble Metal Nanoparticles by Colloidal Atom Clusters—A Kinetic in Situ Study. *J. Colloid Interface Sci.* **2016**, *463*, 299−307.
(25) Poletti, A.; Fracasso, G.; Conti, G.; Pilot, R.; Amendola, V. Laser Generated Gold Nanocorals with Broadband Plasmon Absorption for Photothermal Applications. *Nanoscale* **2015**, *7*, 13702−13714.
(26) Zhou, L.; Zhang, H.; Bao, H.; Liu, G.; Li, Y.; Cai, W. Onion-Structured Spherical MoS_2 Nanoparticles Induced by Laser Ablation in Water and Liquid Droplets' Radial Solidification/Oriented Growth Mechanism. *J. Phys. Chem. C* **2017**, *121*, 23233−23239.
(27) Shih, C.-Y.; Streubel, R.; Heberle, J.; Letzel, A.; Shugaev, M.; Wu, C.; Schmidt, M.; Gokce, B.; Barcikowski, S.; Zhigilei, L. Two mechanisms of nanoparticle generation in picosecond laser ablation in liquids: The origin of the bimodal size distribution. *Nanoscale* **2018**, *10*, 6900−6910.
(28) Zhang, D.; Choi, W.; Oshima, Y.; Wiedwald, U.; Cho, S.-H.; Lin, H.-P.; Li, Y.; Ito, Y.; Sugioka, K. Magnetic Fe@FeO_x, Fe@C and α-Fe_2O_3 Single-Crystal Nanoblends Synthesized by Femtosecond Laser Ablation of Fe in Acetone. *Nanomaterials* **2018**, *8*, No. 631.
(29) Kabashin, A. V.; Meunier, M. Synthesis of Colloidal Nanoparticles during Femtosecond Laser Ablation of Gold in Water. *J. Appl. Phys.* **2003**, *94*, 7941−7943.
(30) Tsuji, T.; Iryo, K.; Watanabe, N.; Tsuji, M. Preparation of Silver Nanoparticles by Laser Ablation in Solution: Influence of Laser Wavelength on Particle Size. *Appl. Surf. Sci.* **2002**, *202*, 80−85.
(31) Menéndez-Manjón, A.; Barcikowski, S. Hydrodynamic Size Distribution of Gold Nanoparticles Controlled by Repetition Rate during Pulsed Laser Ablation in Water. *Appl. Surf. Sci.* **2011**, *257*, 4285−4290.
(32) Yu, J.; Nan, J.; Zeng, H. Size control of nanoparticles by multiple-pulse laser ablation. *Appl. Surf. Sci.* **2017**, *402*, 330−335.
(33) Luo, R.-C.; Li, C.; Du, X.-W.; Yang, J. Direct Conversion of Bulk Metals to Size-Tailored, Monodisperse Spherical Non-Coinage-Metal Nanocrystals. *Angew. Chem., Int. Ed.* **2015**, *54*, 4787−4791.
(34) Lau, M.; Barcikowski, S. Quantification of mass-specific laser energy input converted into particle properties during picosecond pulsed laser fragmentation of zinc oxide and boron carbide in liquids. *Appl. Surf. Sci.* **2015**, *348*, 22−29.
(35) Schaumberg, C. A.; Wollgarten, M.; Rademann, K. Fragmentation Mechanism of the Generation of Colloidal Copper (I) Iodide Nanoparticles by Pulsed Laser Irradiation in Liquids. *Phys. Chem. Chem. Phys.* **2015**, *17*, 17934−17938.
(36) Zhang, D.; Lau, M.; Lu, S.; Barcikowski, S.; Gökce, B. Germanium Sub-Microspheres Synthesized by Picosecond Pulsed Laser Melting in Liquids: Educt Size Effects. *Sci. Rep.* **2017**, *7*, No. 40355.
(37) Luo, T.; Wang, P.; Qiu, Z.; Yang, S.; Zeng, H.; Cao, B. Smooth and solid WS_2 submicrospheres grown by a new laser fragmentation and reshaping process with enhanced tribological properties. *Chem. Commun.* **2016**, *52*, 10147−10150.
(38) Wang, H.; Pyatenko, A.; Kawaguchi, K.; Li, X.; Swiatkowska-Warkocka, Z.; Koshizaki, N. Selective pulsed heating for the synthesis of semiconductor and metal submicrometer spheres. *Angew. Chem.* **2010**, *122*, 6505−6508.
(39) Singh, R.; Soni, R. K. Laser Synthesis of Aluminium Nanoparticles in Biocompatible Polymer Solutions. *Appl. Phys. A* **2014**, *116*, 689−701.
(40) Binaymotlagh, R.; Hadadzadeh, H.; Farrokhpour, H.; Haghighi, F. H.; Abyar, F.; Mirahmadi-Zare, S. Z. In Situ Generation of the Gold Nanoparticles−Bovine Serum Albumin (AuNPs−BSA) Bioconjugated System Using Pulsed-Laser Ablation (PLA). *Mater. Chem. Phys.* **2016**, *177*, 360−370.
(41) Walter, J. G.; Petersen, S.; Stahl, F.; Scheper, T.; Barcikowski, S. Laser Ablation-Based One-Step Generation and Bio-Functionalization of Gold Nanoparticles Conjugated with Aptamers. *J. Nanobiotechnol.* **2010**, *8*, No. 21.
(42) Letzel, A.; Gökce, B.; Wagener, P.; Ibrahimkutty, S.; Menzel, A.; Plech, A.; Barcikowski, S. Size Quenching during Laser Synthesis of Colloids Happens Already in the Vapor Phase of the Cavitation Bubble. *J. Phys. Chem. C* **2017**, *121*, 5356−5365.

DOI: 10.1021/acsomega.8b01250
ACS Omega 2018, 3, 10953−10966

(43) Rehbock, C.; Merk, V.; Gamrad, L.; Streubel, R.; Barcikowski, S. Size control of laser-fabricated surfactant-free gold nanoparticles with highly diluted electrolytes and their subsequent bioconjugation. *Phys. Chem. Chem. Phys.* **2013**, *15*, 3057−3067.
(44) Díaz-Núñez, P.; González-Izquierdo, J.; González-Rubio, G.; Guerrero-Martínez, A.; Rivera, A.; Perlado, J. M.; Bañares, L.; Peña-Rodríguez, O. Effect of Organic Stabilizers on Silver Nanoparticles Fabricated by Femtosecond Pulsed Laser Ablation. *Appl. Sci.* **2017**, *7*, No. 793.
(45) Mafuné, F.; Kohno, J.-y.; Takeda, Y.; Kondow, T.; Sawabe, H. Formation and size control of silver nanoparticles by laser ablation in aqueous solution. *J. Phys. Chem. B* **2000**, *104*, 9111−9117.
(46) Yang, S.; Cai, W.; Zhang, H.; Xu, X.; Zeng, H. Size and Structure Control of Si Nanoparticles by Laser Ablation in Different Liquid Media and Further Centrifugation Classification. *J. Phys. Chem. C* **2009**, *113*, 19091−19095.
(47) Zhang, D.; Choi, W.; Jakobi, J.; Kalus, M.-R.; Barcikowksi, S.; Cho, S.-H.; Sugioka, K. Spontaneous Shape Alteration and Size Separation of Surfactant-Free Silver Particles Synthesized by Laser Ablation in Acetone during Long-Period Storage. *Nanomaterials* **2018**, *8*, No. 529.
(48) Dell'Aglio, M.; Mangini, V.; Valenza, G.; De Pascale, O.; De Stradis, A.; Natile, G.; Arnesano, F.; De Giacomo, A. Silver and Gold Nanoparticles Produced by Pulsed Laser Ablation in Liquid to Investigate Their Interaction with Ubiquitin. *Appl. Surf. Sci.* **2016**, *374*, 297−304.
(49) Amendola, V.; Polizzi, S.; Meneghetti, M. Free Silver Nanoparticles Synthesized by Laser Ablation in Organic Solvents and Their Easy Functionalization. *Langmuir* **2007**, *23*, 6766−6770.
(50) Jiguet, S.; Bertsch, A.; Hofmann, H.; Renaud, P. SU8-Silver Photosensitive Nanocomposite. *Adv. Eng. Mater.* **2004**, *6*, 719−724.
(51) Jiguet, S.; Bertsch, A.; Hofmann, H.; Renaud, P. Conductive SU8 Photoresist for Microfabrication. *Adv. Funct. Mater.* **2005**, *15*, 1511−1516.
(52) Jakobi, J.; Petersen, S.; Menéndez-Manjón, A.; Wagener, P.; Barcikowski, S. Magnetic Alloy Nanoparticles from Laser Ablation in Cyclopentanone and Their Embedding into a Photoresist. *Langmuir* **2010**, *26*, 6892−6897.
(53) Jonušauskas, L.; Lau, M.; Gruber, P.; Gökce, B.; Barcikowski, S.; Malinauskas, M.; Ovsianikov, A. Plasmon Assisted 3D Microstructuring of Gold Nanoparticle-Doped Polymers. *Nanotechnology* **2016**, *27*, No. 154001.
(54) Bhattacharjya, D.; Park, H.-Y.; Kim, M.-S.; Choi, H.-S.; Inamdar, S. N.; Yu, J.-S. Nitrogen-doped carbon nanoparticles by flame synthesis as anode material for rechargeable lithium-ion batteries. *Langmuir* **2013**, *30*, 318−324.
(55) Firoz Babu, K.; Dhandapani, P.; Maruthamuthu, S.; Anbu Kulandainathan, M. One pot synthesis of polypyrrole silver nanocomposite on cotton fabrics for multifunctional property. *Carbohydr. Polym.* **2012**, *90*, 1557−1563.
(56) Hoflund, G. B.; Hazos, Z. F.; Salaita, G. N. Surface characterization study of Ag, AgO, and Ag_2O using x-ray photoelectron spectroscopy and electron energy-loss spectroscopy. *Phys. Rev. B* **2000**, *62*, No. 11126.
(57) Dwivedi, N.; Yeo, R. J.; Satyanarayana, N.; Kundu, S.; Tripathy, S.; Bhatia, C. S. Understanding the Role of Nitrogen in Plasma-Assisted Surface Modification of Magnetic Recording Media with and without Ultrathin Carbon Overcoats. *Sci. Rep.* **2015**, *5*, No. 7772.
(58) Zhang, H.; Zou, G.; Liu, L.; Li, Y.; Tong, H.; Sun, Z.; Zhou, Y. N. A comparative study of silver nanoparticles synthesized by arc discharge and femtosecond laser ablation in aqueous solution. *Appl. Phys. A* **2016**, *122*, No. 896.
(59) Wang, X.; Liu, Y.; Han, H.; Zhao, Y.; Ma, W.; Sun, H. Polyaniline coated Fe_3O_4 hollow nanospheres as anode materials for lithium ion batteries. *Sustainable Energy Fuels* **2017**, *1*, 915−922.
(60) Li, H.-J.; Zhang, A.-Q.; Hu, Y.; Sui, L.; Qian, D.-J.; Chen, M. Large-scale synthesis and self-organization of silver nanoparticles with Tween 80 as a reductant and stabilizer. *Nanoscale Res. Lett.* **2012**, *7*, No. 612.
(61) Chen, H.; Ojijo, V. O.; Cele, H.; Joubert, T.; Ray, S.; Land, K. Tailoring the Mechanical Properties of SU-8/Clay Nanocomposites: Polymer Microcantilever Fabrication Perspective. In *Sensors, MEMS, and Electro-Optical systems*, SPIE Proceedings; Plessis, M., Ed.; International Society for Optics and Photonics, 2014; Vol. *9257*, p 92570B.
(62) Fei, X.; Wan, Y.; Zhang, H.; Cui, Z.; Zhang, D. Synthesis of a fluorinated photoresist for optical waveguide devices. *Appl. Phys. A* **2009**, *96*, 467−472.
(63) Jiang, H.; Moon, K.-S.; Lu, J.; Wong, C. P. Conductivity enhancement of nano silver-filled conductive adhesives by particle surface functionalization. *J. Electron. Mater.* **2005**, *34*, 1432−1439.
(64) Mbhele, Z. H.; Salemane, M. G.; van Sittert, C. G. C. E.; Nedeljković, J. M.; Djoković, V.; Luyt, A. S. Fabrication and Characterization of Silver−Polyvinyl Alcohol Nanocomposites. *Chem. Mater.* **2003**, *15*, 5019−5024.
(65) Rodriguez Ponce, D.; Lozano, K.; Eubanks, T.; Harb, A.; Ferrer, D.; Lin, Y. Thermophysical analysis of SU8-modified microstructures created by visible light lithography. *J. Polym. Sci., Part B: Polym. Phys.* **2010**, *48*, 47−54.
(66) Million, N.; Coger, V.; Wilke, P.; Rehbock, C.; Vogt, P. M.; Pich, A.; Barcikowski, S. Water-based, surfactant-free cytocompatible nanoparticle-microgel-composite biomaterials—rational design by laser synthesis, processing into fiber pads and impact on cell proliferation. *Bionanomaterials* **2017**, *18*, No. 20170004.
(67) Wang, Y.; Pai, J.-H.; Lai, H.-H.; Sims, C. E.; Bachman, M.; Li, G.; Allbritton, N. L. Surface graft polymerization of SU-8 for bio-MEMS applications. *J. Micromech. Microeng.* **2007**, *17*, 1371−1380.
(68) Ye, X.; Kestell, J.; Kisslinger, K.; Liu, M.; Grubbs, R. B.; Boscoboinik, J. A.; Nam, C.-Y. Effects of Residual Solvent Molecules Facilitating the Infiltration Synthesis of ZnO in a Nonreactive Polymer. *Chem. Mater.* **2017**, *29*, 4535−4545.
(69) Hurt, A. P.; Kotha, A. K.; Trivedi, V.; Coleman, N. J. Bioactivity, biocompatibility and antimicrobial properties of a chitosan-mineral composite for periodontal tissue regeneration. *Polimeros* **2015**, *25*, 311−316.
(70) Haber, T.; Schmitt, U.; Emmeluth, C.; Suhm, M. A. Ragout-jet FTIR spectroscopy of cluster isomerism and cluster dynamics: from carboxylic acid dimers to N2O nanoparticles. *Faraday Discuss.* **2001**, *118*, 331−359.
(71) Ghosal, A.; Ahmad, S. High performance anti-corrosive epoxy-titania hybrid nanocomposite coatings. *New J. Chem.* **2017**, *41*, 4599−4610.
(72) Nascimento Filho, A. P.; Silva, M. L. P.; Demarquette, N. R. Polymer Production by Plasma Polymerization of Oxygenated Organic Compounds. *Polimeros* **2002**, *12*, 280−284.
(73) Alhwaige, A. A.; Alhassan, S. M.; Katsiotis, M. S.; Ishida, H.; Qutubuddin, S. Interactions, morphology and thermal stability of graphene-oxide reinforced polymer aerogels derived from star-like telechelic aldehyde-terminal benzoxazine resin. *RSC Adv.* **2015**, *5*, 92719−92731.
(74) Bastús, N. G.; Merkoçi, F.; Piella, J.; Puntes, V. Synthesis of Highly Monodisperse Citrate-Stabilized Silver Nanoparticles of up to 200 nm: Kinetic Control and Catalytic Properties. *Chem. Mater.* **2014**, *26*, 2836−2846.
(75) Wagener, P.; Brandes, G.; Schwenke, A.; Barcikowski, S. Impact of in Situ Polymer Coating on Particle Dispersion into Solid Laser-Generated Nanocomposites. *Phys. Chem. Chem. Phys.* **2011**, *13*, 5120−5126.
(76) Zhang, D.; Chen, F.; Fang, G.; Yang, Q.; Xie, D.; Qiao, G.; Li, W.; Si, J.; Hou, X. Wetting characteristics on hierarchical structures patterned by a femtosecond laser. *J. Micromech. Microeng.* **2010**, *20*, No. 075029.
(77) Zhang, D.; Chen, F.; Yang, Q.; Si, J.; Hou, X. Mutual wetting transition between isotropic and anisotropic on directional structures fabricated by femotosecond laser. *Soft Matter* **2011**, *7*, 8337−8342.
(78) Zhang, D.; Chen, F.; Yang, Q.; Yong, J.; Bian, H.; Ou, Y.; Si, J.; Meng, X.; Hou, X. A simple way to achieve pattern-dependent tunable

DOI: 10.1021/acsomega.8b01250
ACS Omega 2018, 3, 10953−10966

adhesion in superhydrophobic surfaces by a femtosecond laser. *ACS Appl. Mater. Interfaces* **2012**, *4*, 4905−4912.

DOI: 10.1021/acsomega.8b01250
ACS Omega 2018, 3, 10953−10966